The DUBA-SLC7A11-c-Myc axis is critical for stemness and ferroptosis

Yongguang Tao (taoyong@csu.edu.cn)
Central South University https://orcid.org/0000-0003-2354-5321
Zuli Wang
Lianlian Ouyang
Key Laboratory of Carcinogenesis and Cancer Invasion(Central South University, Ministry of Education), Department of Pathology, Central South University
Na Liu
Key Laboratory of Carcinogenesis and Cancer Invasion(Central South University, Ministry of Education), Department of Pathology, Central South University https://orcid.org/0000-0001-5162-3791
Tiansheng Li
Bokang Yan
Chao Mao
Desheng Xiao
Boyi Gan
The University of Texas MD Anderson Cancer Center https://orcid.org/0000-0001-8884-6040
Shuang Liu
Key Laboratory of Carcinogenesis and Cancer Invasion(Central South University, Ministry of Education), Department of Pathology, Central South University https://orcid.org/0000-0002-7206-7277

Article

Keywords: CSCs, ferroptosis, SLC7A11, DUBA, ubiquitination, c-Myc

Posted Date: February 15th, 2023

DOI: https://doi.org/10.21203/rs.3.rs-2395378/v1

Version of Record: A version of this preprint was published at Oncogene on August 3rd, 2023. See the published version at https://doi.org/10.1038/s41388-023-02744-0.

Abstract

Ferroptosis is characterized by the accumulation of lipid peroxidation as a unique iron-dependent cell death. However, the interplay between stemness and ferroptosis remains unknown. Here, we demonstrate that undifferentiated cells are more sensitive to ferroptosis than differentiated cells, and cystine transporter SLC7A11 protein is highly up-regulated by deubiquitinase DUBA in differentiated cells. Additionally, DUBA promotes stemness by deubiquitinating SLC7A11. Moreover, SLC7A11 drastically increases the expression of c-Myc through cysteine, the combination of sorafenib and c-Myc inhibitor EN4 has a synergetic effect on cancer therapy. Together, our results reveal that enhanced stemness increases the susceptibility to ferroptosis, and the DUBA-SLC7A11-c-Myc axis is pivotal for differentiated cancer stem cells (CSCs) resistant to ferroptosis, providing a promised targets to eradicate CSCs through ferroptosis.

Introduction

Cancer stem cells (CSCs), a special cell population initiating tumor, are closely associated with cellular heterogeneity and therapeutic resistance of advanced cancers [1]. Four pluripotent inducers OCT4, SOX2, KLF4, and c-Myc (OSKM) named Yamanaka factors can reprogram somatic cells into induced pluripotent stem cells (iPSCs) which decreases the glutathione-mediated reactive oxygen species (ROS) levels, restrain the DNA damage response [2, 3]. Additionally, MYC enhanced the chemotherapy resistance of breast CSCs by increasing mitochondrial oxidative phosphorylation (OXPHOS) and the production of ROS [4]. Targeting CSCs is a promising strategy to eradicate tumors [5].

As a newly defined regulated cell death in 2012, ferroptosis can be inhibited by eliminating lipid peroxides through Glutathione peroxidase (GPX4), which depends on system xc- (SLC3A2 + SLC7A11) importing cystine. Moreover, depletion of glutathione leads to accumulating ROS and ferroptosis, having the tremendous power to connect other areas of biology and medicine for cancer therapy [6, 7]. Epithelial-mesenchymal transition (EMT) marker ZEB1 and Wnt receptor FZD7 activate the mesenchymal progression of cancer cells and mitigate the sensitivity to conventional therapy, while they increase the sensitivity to ferroptosis [8, 9]. In addition, drug resistant cancer cells are vulnerable to GPX4 inhibition, resulting in ferroptotic death and preventing tumor relapse [10].

Compared to cancer cells, CSCs are addicted to more iron to maintain their self-renewal and plasticity. Given the requirement of iron is different from CSCs and others, it is potentially developed that personalized cancer therapies targeting CSCs for iron-regulated ferroptosis beyond traditional treatments [11].

Therefore, this motivates us to explore the susceptibility of stemness to ferroptosis and its concrete molecular mechanism in the study, which can be considered for effective cancer therapy.

Results

Undifferentiated cells are more sensitive to ferroptosis than differentiated cells

To investigate the sensitivity of stemness to ferroptosis, we first cultured different cancer cells with distinct proportion of side population (SP) cells. SP cells, a specific subgroup existed in most tumours, have the same characteristics stemness [12]. Subsequently, we treated these cells with indicated concentrations of various ferroptosis activators, including erastin directly blocking system Xc- [13] and RSL3 inhibiting GPX4 [14, 15]. Compared to lung cancer cells H1299, liver cancer cells LM3, and breast cancer cells MCF-7, the results showed that A549 cells (Figure 1A), Hep3B cells (Figure 1B), MDA-MB-231 cells (Figure S1A) which possessed a higher percentage of SP cells were more sensitive to erastin through cell viability assays. Similarly, glioma cells U87 and breast cancer cells MDA-MB-231 relative to U251 (Figure S1B) and MCF7 (Figure S1C) respectively were more sensitive to ferroptosis inducer RSL3. Besides, compared to H1299 cells, A549 cells displayed a higher level of lipid ROS when they were exposed to RSL3 simultaneously (Figure S1D). Therefore, it was suggested that stemness enhanced the sensitivity to ferroptosis.

Subsequently, to further verify this result, we successfully cultured A549 cells into oncospheres [16] (Figures 1C) and found stemness-related factors like SOX2 were up-regulated in oncospheres (Figures 1D). Compared to parent cells A549, the data showed that tumor sphere-formed cells (Figure 1E) were more sensitive to erastin and RSL3, whereas this could be rescued by ferroptosis inhibitor ferrostatin-1 (Fer-1). Likewise, compared to Hep3B cells, tumor sphere-formed Hep3B cells (Figures S1E and S1F) were more sensitive to Erastin and RSL3 (Figure S1G).

On the other hand, All-trans Retinoic Acid (ATRA) was utilized to induce the mouse embryonal carcinoma stem cells P19 differentiation [17] and reduced the protein levels of OCT-4 and SOX2 (Figure 1F). We also observed that P19 cells relative to differentiated P19 cells had a lower proportion of cell viability under another system Xc- inhibitor Imidazole Ketone Erastin (IKE) [18] and RSL3 treatment (Figure 1G). Moreover, P19 cells exhibited a higher level of lipid ROS (Figure 1H) when they were exposed to RSL3. Besides, the pictures derived from transmission electron microscopy (TEM) demonstrated that a higher degree of thickened crista and shrunken mitochondria were observed in P19 cells beyond differentiated P19 cells (Figure 1I). And more numbers of the dead cells were observed in P19 cells without ATRA-induced differentiation after IKE and RSL3 treatment (Figure 1J). Consequently, this evidence indicated that differentiated cells increased the resistance to ferroptosis.

Taken together, these results demonstrate that enhanced stemness promotes the sensitivity of cells to ferroptosis different from conventional radiotherapy and chemotherapy. It is possible that targeting ferroptosis provides a promising method for CSCs eradication.

SLC7A11 is up-regulated by DUBA in differentiated cells

Notably, the drug-resistant cells always stay at a mesenchymal state, but they have no sufficient antioxidative ability to oxidants like GPX4 inhibitor [19]. To elucidate the detailed mechanisms that CSCs were sensitive to ferroptosis, we first analyzed the protein expression of lipid peroxidation factors

including SLC7A11, ACSL4, GPX4 and COX2 [20] between the A549 cells and H1299 cells (Figure S2A), and U87 cells and U251 cells (Figure S2B), and found SLC7A11 was up-regulated in H1299 cells and U251 cells. Moreover, we treated P19 cells (Figure S2C) and LM3 cells (Figure S2D) with ATRA and found that the mRNA levels of these ferroptosis-related factors have a slight decrease in differentiated cells. This could be explained by two reasons: low levels of ROS could maintain the growth of ATRA-induced cells [21] and the decrease of stemness factors like SOX2 reduced the mRNA levels of SLC7A11 [22]. However, ATRA greatly increased the protein level of SLC7A11 with increasing concentrations of ATRA in P19 cells (Figure 2A) and LM3 cells (Figure 2B), which probably played a vital role in differentiated cells resistant to ferroptosis.

For the protein of SLC7A11 was dramatically up-regulated in differentiated cells, we wondered whether the critical posttranslational modification ubiquitin-proteasome system (UPS) involved this quality control of proteins [23]. To confirm that SLC7A11 protein was regulated by UPS, we treated ATRA-induced P19 cells (Figure 2C) and LM3 cells (Figure 2D) with MG132 respectively. The results demonstrated that MG132 could offset the difference of SLC7A11 protein between DMSO and ATRA treatment, suggesting that SLC7A11 was regulated by UPS in differentiated cells.

Protein ubiquitination which was reversed by several distinct families of deubiquitinases (DUBs) involved in this stabilization process [24]. To screen the DUBs up-regulating SLC7A11, about 90 DUBs including five families: UCHs, USPs, OTUs, Josephins, and JAMMs in the human proteome [25, 26] were transiently transfected into 293T cells. Immunoblotting assays showed that the increasing level of SLC7A11 was the most obvious when DUBA was overexpressed (Figure 2E). Moreover, we detected the protein levels of DUBA in ATRA-induced P19 cells and found that DUBA was increased with increasing concentrations of ATRA (Figure 2F), indicating that ATRA could increase SLC7A11 through inducing DUBA. DUBA is a significant regulator of multiple factors including mTOR signaling, type I interferon and TRAF3 [27].

Iron is mainly stored in liver and the imbalance of iron homeostasis involves various liver diseases including liver injury and hepatocellular carcinoma (HCC) [28]. HCC is one of the leading causes of cancer-related death worldwide [29, 30]. The report points out that triggering ferroptosis in iron-rich tumors (such as HCC and NSCLC, etc) may develop new therapeutic avenues or reverse drug-resistance in cancers [31]. Therefore, HCC cells were considered as main research object in our study. First, we detected the protein levels of DUBA and SLC7A11 in HCC cell lines and found that they both were highly expressed in HCC cell lines relative to normal liver cells 7701. Moreover, there was a positive correlation between DUBA and SLC7A11 in these cell lines (Figure S3A). Subsequently, a similar finding that the SLC7A11 was gradually up-regulated with increasing amounts of DUBA was also observed in Hep3B cells (Figure 2G).

In summary, we discover that SLC7A11 is up-regulated by DUBA in differentiated cells, leading to inhibit cell ferroptosis. This may provide therapy strategy for CSCs through DUBA-SLC7A11.

DUBA stabilizes and interacts with SLC7A11

Next, to investigate the interaction between DUBA and SLC7A11, we first co-transfected DUBA and SLC7A11 into 293T cells and found DUBA could be immunoprecipitated by SLC7A11 antibody (Figure 3A). Moreover, it was also indicated that DUBA was immunoprecipitated by SLC7A11 antibody from LM3 cell lysates (Figure 3B). In addition, the 293T cells were co-transfection with SLC7A11 and DUBA and followed by immunofluorescence assay. The images displayed that there was a co-location between SLC7A11 and DUBA (Figure 3C).

To determine whether DUBA stabilized SLC7A11 protein through deubiquitination, we first treated the DUBA-overexpressed Hep3B cells with the proteasome inhibitor MG132 [32]. The immunoblot displayed that DUBA overexpression increased the level of SLC7A11, whereas there was no obvious difference between Vector and Overexpression cells treated with MG132 (Figure 3D). Furthermore, we treated Hep3B cells overexpressing DUBA using protein synthesis inhibitors cycloheximide (CHX) and examined SLC7A11 protein degradation for the indicated hours. It was indicated that DUBA had a stable effect on SLC7A11 protein (Figure 3E). Conversely, knocking down DUBA with two separate short hairpin RNAs (shRNAs) promoted SLC7A11 degradation in LM3 cells treated with CHX for the indicated hours (Figure 3F).

Above all, we screen and identify a DUBs DUBA that can maintain SLC7A11 stability through deubiquitination through interacting with SLC7A11.

DUBA deubiquitinates SLC7A11

To examine the possibility that DUBA deubiquitinated SLC7A11, *in vitro* ubiquitylation assays showed that DUBA could directly remove the ubiquitin chain of SLC7A11 in Hep3B cells (Figure 4A) and HepG2 cells (Figure 4B). Since different ubiquitin chains have diverse roles in regulating protein location and function [33], we next co-transfected 293T cells with SLC7A11, Ub or its site mutants, and Vector or DUBA to investigate the type of SLC7A11 ubiquitination mediated by DUBA. The results exhibited that DUBA could significantly reduce the ubiquitination level of SLC7A11 in 293T cells transfected with WT ubiquitin and its mutant K48 (Figure 4C), suggesting that DUBA cleaved the K48-linked ubiquitination of SLC7A11 rather than other forms of polyubiquitin chains.

Subsequently, we constructed two different DUBA mutations including a phosphosite mutant DUBA S177A and a catalytic cysteine mutant DUBA C224S [34] and respectively transfected them into Hep3B cells. Immunoblot showed that DUBA S177A and DUBA C224S relative to DUBA wild type (WT) could not up-regulate SLC7A11 dramatically (Figure 4D). Moreover, the cell lysates from 293T cells co-transfected DUBA WT, DUBA S177A, or DUBA C224S with SLC7A11 were precipitated by anti-flag antibody. Consequently, both the two mutations of DUBA did not affect the interaction with SLC7A11 (Figure 4E). However, the ubiquitylation results indicated that DUBA C224S could not evidently decrease the ubiquitination level of SLC7A11 in 293T cells, while DUBA S177A did not affect the ubiquitination level (Figure 4F).

Taken together, these studies corroborate that DUBA can interact and stabilize SLC7A11 through removing the K48-linked ubiquitin chains of SLC7A11, but DUBA C224S could not decrease the ubiquitination level of SLC7A11 relative to DUBA WT, which provides multiple intervention measures for the stabilization of SLC7A11 through DUBA.

DUBA inhibits ferroptosis and enhances stemness

Since the critical role of SLC7A11 in ferroptosis, we confirmed the similar function of DUBA on ferroptosis. Consequently, we found that overexpression of DUBA could resist RSL3 treatment in Hep3B cells (Figure S4A) and decrease the lipid ROS level of Hep3B cells (Figure S4B). Reversely, when DUBA was inhibited in LM3 cells, DUBA inhibition could enhance the sensitivity of cells to ferroptosis (Figure S4C) and increase the lipid ROS level of LM3 cells (Figure S4D).

To explore the role of SLC7A11 in cancer stemness, we found that SLC7A11 overexpression facilitated the oncosphere formation ability of Hep3B cells (Figure S5A). Moreover, SLC7A11 also increased the proportion of SP cells (Figure S5B) and CD338+ cells (Figure S5C) in Hep3B cells, and CD338+ cells population in HepG2 cells (Figure S5D). Then, we investigated the effect of SLC7A11 on key stemness factors (Figure S5E) and surprisingly found that its overexpression up-regulated c-Myc evidently and had a little effect on SOX2 expression, etc. Conversely, the ALDH activity was reduced in LM3 cells (Figure S5F) after the knockdown of SLC7A11 with two shRNAs. This problem that the up-regulation of SLC7A11 promotes cancer stemness in differentiated cells seems contradictory. We consider that SLC7A11 is not a core stemness factor and cannot change the ATRA-induced differentiation. Moreover, the combination of stemness inhibitor and SLC7A11 may show a great therapeutic potential.

To demonstrate the role of DUBA in stemness maintenance, it was found that overexpression of DUBA promoted cell proliferation (Figure S6A) and facilitated sphere formation frequency (Figure 5A) in Hep3B cells. Subsequently, we found that the ALDH activity (Figure 5B) and the proportion of SP cells (Figure 5C) and CD338+ cells (Figure S6B) were increased in Hep3B cells after overexpression of DUBA. Similarly, overexpression of DUBA greatly up-regulated the protein level of c-Myc (Figure 5D). Consistent with the results from *in vitro* experiments, and *in vivo* study indicated that overexpression of DUBA increased incidence of Hep3B xenograft tumor and tumor weight in nude mice subcutaneously injecting Hep3B cells (Figure 5E). Moreover, immunoblot analysis of Hep3B xenograft tumor also displayed that there was a positive correlation between DUBA, SLC7A11, and c-Myc (Figure 5F). Furthermore, we explored the role of DUBA mutations in stemness maintenance and demonstrated that DUBA S177A and DUBA C224S relative to DUBA WT could not promote the growth of HepG2 cells (Figure S6C). Compared to DUBA WT, the ALDH activity (Figure S6D) and the percentage of CD338+ positive cells (Figure 5G) were decreased by DUBA S177A and DUBA C224S in HepG2 cells.

Conversely, the growth (Figure S7A) and migration (Figure S7B) ability of LM3 cells were evidently attenuated when DUBA was inhibited. Moreover, the proportion of SP cells was reduced in LM3 cells after the knockdown of DUBA (Figure S7C). Consistently, we performed LM3 xenograft tumor into nude mice with subcutaneous injection of LM3 cells and found that knockdown of DUBA significantly reduced

tumor size (Figure S7D) and weight (Figure S7E). immunoblot analysis of LM3 xenograft tumor also demonstrated DUBA could stabilize SLC7A11 and c-Myc (Figure S7F).

To sum up, similar to SLC7A11, DUBA inhibits cell ferroptosis and promotes cancer stemness properties both *in vitro* and *in vivo*, while DUBA S177A and DUBA C224S are unable to achieve. DUBA has critical roles in ferroptosis and stemness through SLC7A11 and serves as a promising cancer therapy target.

The DUBA-SLC7A11-c-Myc axis enhances stemness and predicts a poor prognosis in HCC Patients.

To better confirm the DUBA-SLC7A11-c-Myc axis in stemness maintenance, we transfected SLC7A11 into LM3 cells with knockdown of DUBA. The results indicated that DUBA knockdown decreased the level of SLC7A11 and c-Myc (Figure 6A) and inhibited the clone forming ability and metastatic potential (Figure 6B) of LM3 cells were consistent with previous research. Moreover, SLC7A11 overexpression could reverse the status and had no effect on the protein level of DUBA, but significantly increased the protein level of c-Myc.

Since the effect that self-renewal of cells was inhibited by reduced expression of c-Myc-HIF-2α was blocked by N-acetyl cysteine (NAC) [35], we speculated that SLC7A11 could stabilize c-Myc through cysteine. Thus, we cultured LM3 cells (Figure 6C) and HepG2 cells (Figure S8A) with DMEM medium lacking cystine [36] for the indicated hours respectively. As expected, it was found that deprivation of cystine greatly increased the expression of c-Myc at 24 hours and reduced the protein level of c-Myc significantly rather than other stemness factors at 48 hours of treatment. Actually, this change was in accord with a previous study that c-Myc directly or indirectly regulated the expression of amino acid transporters at high levels, especially SLC7A11 and SLC1A5 [37]. Furthermore, the deficiency of cysteine dramatically inhibited LM3 cells growth (Figure S8B) and promoted the sensitivity to RSL3 inducer, which was blocked by the addition of cysteine (Figure S8C). Next, we explored the role of cysteine in stemness via c-Myc. The results showed that ALDH intensity (Figure 6D) was greatly inhibited and the SP population of LM3 cells was decreased when cysteine was deprived in medium (Figure S8D).

To clarify the significance of DUBA and SCL7A11 in HCC patients, we first utilized IHC analysis (Figure 6E) and western blot (Figure 6F) to detect their expression in HCC patient tissues compared to paracancerous normal tissues. The results indicated that both DUBA and SLC7A11 were increased in HCC samples relative to normal samples. Next, Kaplan–Meier curves analysis was used to estimate the relationship between the level of DUBA and SLC7A11 and the survival rate of HCC patients. According to the TCGA database, we found that high expression of DUBA and SLC7A11 was in accord with a low survival rate respectively (Figure 6G). Moreover, the combined high expression of DUBA and SLC7A11 predicted a lower survival ratio relative to the collectively low expression of them (Figure 6H).

In a word, SLC7A11 is up-regulated by DUBA through deubiquitination and imported cystine stabilizing c-Myc protein mainly, thus resisting ferroptosis and enhancing stemness. Moreover, both DUBA and SLC7A11 are highly expressed in HCC patients, and their combined high expression predicts a poor prognosis.

The combined treatment of sorafenib and c-Myc inhibitor EN4 inhibits HCC.

Currently, though sorafenib is the only first-line chemotherapy for advanced HCC, it is far from satisfactory in HCC therapy efficacy and causes severe adverse effects [38, 39]. Besides, sorafenib could induce HCC cells ferroptosis through SLC7A11 inhibition [40]. Thus, to investigate the effect of DUBA on sorafenib treatment, we first treated DUBA-overexpressed Hep3B cells with sorafenib and found that overexpression of DUBA could enhance the growth inhibition (Figure 7A) and tumorspheres formation (Figure 7B), while DUBA S177A and DUBA C224S could not resist to sorafenib. Conversely, after exposure to sorafenib, the knockdown of DUBA greatly restrained LM3 cell proliferation (Figure S9C) and oncospheres formation (Figure S9D) beyond without sorafenib.

For the stability of c-Myc by SLC7A11, a c-Myc inhibitor EN4 [41] was used to treat HCC in combination with sorafenib. First, we treated Hep3B cells with EN4 and found that DUBA could enhance the growth inhibition (Figure 7C). To determine the significance of combination between sorafenib and EN4 in HCC, we first co-treated LM3 cells with EN4 and sorafenib. The results uncovered that their combination had an obvious growth inhibition beyond EN4 or sorafenib alone (Figure 7D) and decreased ALDH intensity dramatically (Figure 7E). Moreover, compared to EN4 or sorafenib treatment, the combination of sorafenib and EN4 significantly increased the lipid ROS level of LM3 cells (Figure 7F). Importantly, the sorafenib or EN4 had no effect on the expression of SLC7A11 and c-Myc separately, while their combination significantly decreased the level of SLC7A11 and c-Myc (Figure 7G).

Above all, we demonstrate an important pathway DUBA-SLC7A11-c-Myc increases the resistance to sorafenib and EN4. Moreover, the combination of sorafenib and EN4 has a synergetic inhibition role in HCC progression through stemness maintenance and ferroptosis, which could be a new and effective treatment modality for HCC (Figure 7H).

Discussion

Since the CSCs are responsible for cancer metastasis, recurrence, and heterogeneity that seriously threaten human life, chemotherapy, radiotherapy, and targeted therapy are failed to eradicate tumors [42]. Stem cells generally share two pivotal abilities to self-renew indefinitely and differentiate into diverse cell types. Thus, exploring the control of embryonic stem cells, adult stem cells, and CSCs function may guide our understanding of human disease and tissue homeostasis and cancer grade and metastasis [43]. For example, pharmacologic targeting of circadian networks induced apoptosis which disrupted cancer stem cell growth [44]. On the other hand, impaired cancer cell stemness results in increased apoptosis and reduced survival potential [45]. Especially, two different research institutions recently have revealed chaperone-mediated autophagy (CMA) not only sustains hematopoietic stem-cell pluripotency [46], but embryonic stem cell's function. Moreover, CMA is up-regulated in these activated cells [47]. In addition, current studies have indicated that high intracellular iron content is required for CSCs growth, and targeting ferroptosis can induce CSCs death [48]. Ferroptosis plays a significant role in radiotherapy-

triggered and chemotherapy-caused cell death in tumor suppression [49]. Thus, combination therapeutic strategies of ferroptosis targeting CSCs are the promising way to effective cancer treatment.

In our study, we have demonstrated that enhanced stemness increases the sensitive of cells to ferroptosis and infer that the lack of antioxidant ability and the abundance of iron storage make CSCs sensitive to ferroptosis. Moreover, SLC7A11 protein is stabilized by DUBA via deubiquitination in differentiated cells. And the stabilizing efficiency of DUBA on SLC7A11 is greater than OTUB1 reported previously [50]. However, their binding sites remain to be investigated and the inhibitors of DUBA have not been developed. In addition, DUBA-SLC7A11 enhances the stem cell-like properties by increasing the level of c-Myc. About the problems that SLC7A11 is up-regulated in differentiated cells and promotes cell stemness, we suppose that SLC7A11 is not a core stemness factors and cannot change the state of differentiated cells. If the cancer cells are treated with SLC7A11 overexpression and differentiation inducers like ATRA, they are more resistant to ferroptosis. As a critical role in innate immune and T cells [51], DUBA not only increases the resistance of cells to sorafenib, but also to c-Myc inhibitor EN4. Importantly, the combination of sorafenib and EN4 greatly promotes ferroptosis and attenuates stemness, displaying a synergetic inhibition role in HCC progression.

Since the pluripotency of stem cells is determined by the core stemness factors, like SOX2 and Nanog, their regulations of them play an essential role in stemness maintenance. Recently, besides transcriptional and epigenetic regulation, extensive researches declared that post-translational modifications are also an important way to maintain stemness, especially ubiquitination [52]. For instance, OTUD7B increases the stability of SOX2 by removing polyUb from it during neural progenitor cells (NPCs) differentiation [53]. Conversely, Ube2s ubiquitinates and degrades SOX2 through the proteasomal system, which contributes to mouse ES cell maintenance [54]. In our study, we demonstrate that SLC7A11 also could be a critical stemness maintenance factor and identified deubiquitinase DUBA on SLC7A11 stability. Moreover, apart from transcriptional regulation like deubiquitinase BAP1 and P53 [55], the Gan professor proposes that the diverse post-translational mechanisms of SLC7A11 can be a meaningful strategy for ferroptosis, nutrient dependency, and cancer therapy [56]. In addition, we demonstrated that cysteine mediated by SLC7A11 had a more stable effect on c-Myc than SOX2 and KLF4, which enhanced the stem cell-like properties distinctly.

To sum up, we demonstrate the interplay between stemness and ferroptsis, and uncover the potential molecular mechanism. Based on the critical role of DUBA in ferroptosis and immune, we hope to combine DUBA inhibitor and conventional therapy targeting ferroptosis for CSCs elimination, providing a promising strategy for effective cancer therapy.

Material And Methods

Cell culture

Human normal hepatocytes 7701, human hepatoma cell lines Hep3B, HepG2, LM3 and 7721, mouse embryonal carcinoma cells P19 and 293T Cells were obtained from the Cancer Research Institute of

Central South University. All these cells were cultured in DMEM medium (Gibco, USA) supplemented with 10%FBS and maintained at 37°C with 5% CO2. DMEM medium lacking glutamine, methionine, and cystine were purchased from Gibco (Cat#21013024).

Chemicals

Erastin (Cat#S7242), RSL3 (Cat#S7242), Fer-1 (Cat#S7243), and ATRA (Cat#S1653) were purchased from Selleck. Sorafenib (Cat#T0093L) and EN4 MYC inhibitor (Cat#T9061) were purchased from TOPSCIENCE.

Plasmids

SLC7A11 cDNA clones were purchased from Vigene Biosciences. DUBA and DUB plasmids were obtained from Peking University. Sequences for DUBA shRNA#1 and shRNA#2 are as follows: 5'-AGGACTTTACCACCTACATTA-3', 5'-ACAACAGTGAGGACGAGTATG-3'. The transfection of plasmids was performed using LipoMax (SUDGEN), and stably expressing cells were selected using 1 mg/ml puromycin.

Cell viability assays

1×10^3 cells were seeded in DMEM medium (100μl/well) into 96 well plates with five replicate wells. After an overnight incubation, each well was added into 10 μl Cell Counting Kit-8 (Bimake) and incubated at 37 °C 5% CO2 for 2h. Absorption values were measured at 450 nm on a multiple-well plate reader (Bio-Tek) and at 48h. The cell viability was expressed as A/B, where A was the absorbance value from the experimental group and B was that from the control cells.

Quantitative real-time PCR (qRT-PCR)

Primers are listed in Supplementary Tables S1. TRIzol reagent (Takara) was used to separate total RNA. PrimeScriptTM RT reagent kit (Takara) was utilized to generate cDNA. Real-time PCR was analyzed by FastStart Universal SYBR Green Master. Relative gene expression was standardized by β-actin.

Western blot

Cells were harvested and washed twice with 1×PBS, lysed in IP lysis buffer on the ice for 2 hours. After centrifugation at 15,000 × g, 4℃ for 15 min, a quantity of 50 μg total protein was used for Western blot analysis. The protein lysates were resolved on SDS-PAGE gels and transferred onto a PVDF transmembrane for 2 hours. The membrane was incubated at 4℃ overnight with different primary antibodies. The next day, after washing three times with PBST, the membrane was incubated at room temperature with a corresponding second antibody and exposed by ChemiDox XRS+ image-forming system.

Immunoprecipitation

Total proteins were extracted in cell lysis buffer supplemented with protease inhibitor cocktail (MCE). Soluble cell lysates (1mg protein) were pre-cleared with 5μl protein G magnetic beads (Invitrogen) for 2h at 4°C. Protein G magnetic beads were removed, followed by incubation at 4°C with another 5μl protein G magnetic beads with antibodies overnight. Unbound proteins were removed by washing three times with lysis buffer. Following SDS-PAGE, immunoprecipitated proteins were transferred onto PVDF membranes and probed with various antibodies.

Immunofluorescence

Cells were fixed with pre-cooled methanol and permeabilized with 0.2% (vol/vol) Triton X-100 for 20 min at room temperature. Cells were blocked with 1% (vol/vol) BSA-PBS solution for 1h at room temperature and incubated with primary antibody (1:500) at 4°C overnight. The secondary antibody (1:2000) was diluted in 1% (vol/vol) BSA-PBS and incubated at room temperature for 1 h. The slides were counterstained with DAPI. The slides were imaged using a Leica confocal microscope. The antibodies used were, anti-mouse Alexa Fluor 594, and anti-rabbit Alexa Fluor 488 (Invitrogen).

Transmission electron microscopy

P19 cells were seeded onto 6 cm plates and were treated with 10 μM erastin for 48 hours. And the cells were fixed with 2.5% Glutaraldehyde solution. Images were acquired using a transmission electron microscope (HITACHI, HT7700).

Total Lipid ROS

The details of these procedures have been described previously [57].

For Lipid ROS determination, cells were added 10μM C11-BODIPY (Thermo Fisher, Cat#D3861) probe. More than 20 000 cells were analyzed by a flow cytometer (BD Biosciences) with FITC-green channel and Texas-red channel.

Tumor sphere formation

Tumor sphere formation analysis was conducted as described before. In short, cells were plated in ultra-low attachment six-well plates (Corning) and were cultured in serum-free DMEM-F12 medium, supplemented with B-27 supplement (Gibco), 20 ng/ml EGF (Sigma), 20 ng/ml b-FGF (Gibco) as well as N-2 Plus Media Supplement (Gibco). After culturing for 1–2 weeks at 37 °C with 5% CO2, cells then formed floating tumorspheres. Eventually, spheres larger than 50 μm in diameter were counted and analyzed.

Aldefluor assay, SP analysis, and CD338 activity

The details of these procedures have been described previously [58]. The Aldefluor assay (STEMCELL Technologies) was performed by the manufacturer's instructions and analyzed with FlowJo software.

For SP analysis, the cells were harvested, resuspended at 1 × 10^6 cells/ml in PBS buffer containing 2% FBS, and Hoechst 33342 was added at a final concentration of 5 μg/ml with or without 50 μM Verapamil (Sigma), which was used to inhibit ABC transporters, followed by incubating at 37 °C for 90 min. Then, the cells were washed with ice-cold PBS buffer and re-suspended with ice-cold PBS buffer containing 2% FBS. Ultimately, propidium iodide was added to the cell suspension at a final concentration of 1-2 μg/ml (PI, Sigma).

The SP cells were selected and sorted by FACS and analyzed with FlowJo software.

Immunohistochemistry (IHC)

The Department of Pathology at Xiangya Hospital verified and provided biopsies of lung cancer. The method used for IHC analysis of paraffin sections from lung cancer tissues can be found in previous literature. Differential quantification was performed by two pathologists from Xiangya Hospital, Changsha, China.

Nude mice and study approval

The 4-week-old female nude mice were purchased from Hunan SJA Laboratory Animal Co., Ltd. (Changsha, China) and were subcutaneously injected with 1×10^6 cells. Tumor volume and the body weight of the nude mice were supervised. After 28 days, the tumors were removed after the mice were sacrificed at the indicated time, and then the weight of tumors was calculated.

All experimental procedures for animal study were approved by the Institutional Animal Care and Use Committee of the Xiangya Hospital (No.2020sydw0117), Central South University and adhered to the legal mandates and national guidelines for animal care and maintenance.

Statistical analyses

All statistical analyses were performed using the Graphpad Prism 8.0 software package (Abbott Laboratories, USA) for Windows. The data are presented as mean ± SEM from multiple individual experiments each performed in triplicates. Student's t-tests (two-tailed) were applied to compare differences between two groups: ns is non-significant ($P > 0.05$), *$P < 0.05$, **$P < 0.01$, ***$P < 0.001$.

Abbreviations

CSCs, cancer stem cells; SP, side population; ATRA, All-trans Retinoic Acid; DUBs, deubiquitinases; TEM, transmission electron microscopy; iPSCs, induced pluripotent stem cells; ROS, reactive oxygen species; OXPHOS, oxidative phosphorylation; EMT, Epithelial-mesenchymal transition; GPX4, Glutathione peroxidase; qRT-PCR, Quantitative real-time PCR; IHC, Immunohistochemistry; IKE, Imidazole Ketone Erastin.

Declarations

Acknowledgments

We thank Xiaoying Wu and Jin Lin at the Central South University for technical assistance with Transmission electron microscopy. We appreciate Lingqiang Zhang at Peking University for assistance with 89 DUB plasmids. We thank all the members of the laboratory for their resourceful comments on the manuscript. This work was supported by the National Natural Science Foundation of China [82072594, YT; 82073097, 81874139 S.Liu; 82073136, 81772927, DX; 82002916, CM], China Postdoctoral Science Foundation [2019M652804, CM], Natural Science Foundation of Hunan Province [2020JJ5790, CM], Hunan Provincial Key Area R&D Programs [2021SK2013, YT].

Author contributions

In this study, Y.T. and Z.W. designed the experimental scheme and drafted the manuscript. Z.W. performed the experiments and data analysis. N.L. and L.O. assisted with stemness-related experiments. B.Y. and T.L. help with preparation for experimental materials. S.L. provided help for FACS and D.X provided help for IHC and modified the original paper. The paper was approved by all authors.

Declaration of interests

The authors declare no competing interests.

Data availability

The data that support the findings of this study are available from the corresponding author upon reasonable request.

References

1. Bayik, D. and J.D. Lathia, *Cancer stem cell-immune cell crosstalk in tumour progression.* Nat Rev Cancer, 2021. **21**(8): p. 526-536.
2. Chronis, C., et al., *Cooperative Binding of Transcription Factors Orchestrates Reprogramming.* Cell, 2017. **168**(3): p. 442-459 e20.
3. Skamagki, M., et al., *Author Correction: ZSCAN10 expression corrects the genomic instability of iPSCs from aged donors.* Nat Cell Biol, 2019. **21**(4): p. 531-532.
4. Lee, K.M., et al., *MYC and MCL1 Cooperatively Promote Chemotherapy-Resistant Breast Cancer Stem Cells via Regulation of Mitochondrial Oxidative Phosphorylation.* Cell Metab, 2017. **26**(4): p. 633-647 e7.
5. Wang, C., et al., *CD276 expression enables squamous cell carcinoma stem cells to evade immune surveillance.* Cell Stem Cell, 2021. **28**(9): p. 1597-1613 e7.
6. Stockwell, B.R., et al., *Ferroptosis: A Regulated Cell Death Nexus Linking Metabolism, Redox Biology, and Disease.* Cell, 2017. **171**(2): p. 273-285.

7. Wang, Z., et al., *A Nuclear Long Non-Coding RNA LINC00618 Accelerates Ferroptosis in a Manner Dependent upon Apoptosis.* Mol Ther, 2021. **29**(1): p. 263-274.
8. Lee, J., et al., *Epigenetic reprogramming of epithelial-mesenchymal transition promotes ferroptosis of head and neck cancer.* Redox Biol, 2020. **37**: p. 101697.
9. Wang, Y., et al., *Frizzled-7 Identifies Platinum-Tolerant Ovarian Cancer Cells Susceptible to Ferroptosis.* Cancer Res, 2021. **81**(2): p. 384-399.
10. Hangauer, M.J., et al., *Drug-tolerant persister cancer cells are vulnerable to GPX4 inhibition.* Nature, 2017. **551**(7679): p. 247-250.
11. El Hout, M., et al., *A promising new approach to cancer therapy: Targeting iron metabolism in cancer stem cells.* Semin Cancer Biol, 2018. **53**: p. 125-138.
12. Zhong, Q., et al., *The RARS-MAD1L1 Fusion Gene Induces Cancer Stem Cell-like Properties and Therapeutic Resistance in Nasopharyngeal Carcinoma.* Clin Cancer Res, 2018. **24**(3): p. 659-673.
13. Wang, M., et al., *Correction to: Long noncoding RNA LINC00336 inhibits ferroptosis in lung cancer by functioning as a competing endogenous RNA.* Cell Death Differ, 2020. **27**(4): p. 1447.
14. Dixon, S.J., et al., *Ferroptosis: an iron-dependent form of nonapoptotic cell death.* Cell, 2012. **149**(5): p. 1060-72.
15. Mao, C., et al., *A G3BP1-Interacting lncRNA Promotes Ferroptosis and Apoptosis in Cancer via Nuclear Sequestration of p53.* Cancer Res, 2018. **78**(13): p. 3484-3496.
16. Liu, N., et al., *The cross-talk between methylation and phosphorylation in lymphoid-specific helicase drives cancer stem-like properties.* Signal Transduct Target Ther, 2020. **5**(1): p. 197.
17. Hou, Z., et al., *LIM protein Ajuba functions as a nuclear receptor corepressor and negatively regulates retinoic acid signaling.* Proc Natl Acad Sci U S A, 2010. **107**(7): p. 2938-43.
18. Ye, L.F., et al., *Radiation-Induced Lipid Peroxidation Triggers Ferroptosis and Synergizes with Ferroptosis Inducers.* ACS Chem Biol, 2020. **15**(2): p. 469-484.
19. Stockwell, B.R., X. Jiang, and W. Gu, *Emerging Mechanisms and Disease Relevance of Ferroptosis.* Trends Cell Biol, 2020. **30**(6): p. 478-490.
20. Zhang, Z., et al., *RNA-binding protein ZFP36/TTP protects against ferroptosis by regulating autophagy signaling pathway in hepatic stellate cells.* Autophagy, 2020. **16**(8): p. 1482-1505.
21. Cabezas-Wallscheid, N., et al., *Vitamin A-Retinoic Acid Signaling Regulates Hematopoietic Stem Cell Dormancy.* Cell, 2017. **169**(5): p. 807-823 e19.
22. Wang, X., et al., *Stem Cell Factor SOX2 Confers Ferroptosis Resistance in Lung Cancer via Upregulation of SLC7A11.* Cancer Res, 2021. **81**(20): p. 5217-5229.
23. Pohl, C. and I. Dikic, *Cellular quality control by the ubiquitin-proteasome system and autophagy.* Science, 2019. **366**(6467): p. 818-822.
24. Harrigan, J.A., et al., *Deubiquitylating enzymes and drug discovery: emerging opportunities.* Nat Rev Drug Discov, 2018. **17**(1): p. 57-78.

25. Ouyang, L., et al., *The deubiquitylase UCHL3 maintains cancer stem-like properties by stabilizing the aryl hydrocarbon receptor.* Signal Transduct Target Ther, 2020. **5**(1): p. 78.
26. Yuan, L., et al., *Deubiquitylase OTUD3 regulates PTEN stability and suppresses tumorigenesis.* Nat Cell Biol, 2015. **17**(9): p. 1169-81.
27. Rutz, S., et al., *Deubiquitinase DUBA is a post-translational brake on interleukin-17 production in T cells.* Nature, 2015. **518**(7539): p. 417-21.
28. Chen, S., et al., *The Emerging Role of Ferroptosis in Liver Diseases.* Front Cell Dev Biol, 2021. **9**: p. 801365.
29. Nakayama, J. and Z. Gong, *Transgenic zebrafish for modeling hepatocellular carcinoma.* MedComm (2020), 2020. **1**(2): p. 140-156.
30. Klein, I.A., et al., *Partitioning of cancer therapeutics in nuclear condensates.* Science, 2020. **368**(6497): p. 1386-1392.
31. Hu, W., et al., *FTH promotes the proliferation and renders the HCC cells specifically resist to ferroptosis by maintaining iron homeostasis.* Cancer Cell Int, 2021. **21**(1): p. 709.
32. Chen, L., et al., *DNA methylation modifier LSH inhibits p53 ubiquitination and transactivates p53 to promote lipid metabolism.* Epigenetics Chromatin, 2019. **12**(1): p. 59.
33. Guo, Y., et al., *OTUD5 promotes innate antiviral and antitumor immunity through deubiquitinating and stabilizing STING.* Cell Mol Immunol, 2021. **18**(8): p. 1945-1955.
34. Huang, O.W., et al., *Phosphorylation-dependent activity of the deubiquitinase DUBA.* Nat Struct Mol Biol, 2012. **19**(2): p. 171-5.
35. Das, B., et al., *MYC Regulates the HIF2alpha Stemness Pathway via Nanog and Sox2 to Maintain Self-Renewal in Cancer Stem Cells versus Non-Stem Cancer Cells.* Cancer Res, 2019. **79**(16): p. 4015-4025.
36. Badgley, M.A., et al., *Cysteine depletion induces pancreatic tumor ferroptosis in mice.* Science, 2020. **368**(6486): p. 85-89.
37. Bhutia, Y.D., et al., *Amino Acid transporters in cancer and their relevance to "glutamine addiction": novel targets for the design of a new class of anticancer drugs.* Cancer Res, 2015. **75**(9): p. 1782-8.
38. Jian, C., et al., *Low-Dose Sorafenib Acts as a Mitochondrial Uncoupler and Ameliorates Nonalcoholic Steatohepatitis.* Cell Metab, 2020. **31**(5): p. 892-908 e11.
39. Yuan, H., et al., *SETD2 Restricts Prostate Cancer Metastasis by Integrating EZH2 and AMPK Signaling Pathways.* Cancer Cell, 2020. **38**(3): p. 350-365 e7.
40. Gao, R., et al., *YAP/TAZ and ATF4 drive resistance to Sorafenib in hepatocellular carcinoma by preventing ferroptosis.* EMBO Mol Med, 2021. **13**(12): p. e14351.
41. Boike, L., et al., *Discovery of a Functional Covalent Ligand Targeting an Intrinsically Disordered Cysteine within MYC.* Cell Chem Biol, 2021. **28**(1): p. 4-13 e17.
42. Yang, L., et al., *Targeting cancer stem cell pathways for cancer therapy.* Signal Transduct Target Ther, 2020. **5**(1): p. 8.

43. Saba, J.A., et al., *Translational control of stem cell function.* Nat Rev Mol Cell Biol, 2021. **22**(10): p. 671-690.
44. Dong, Z., et al., *Targeting Glioblastoma Stem Cells through Disruption of the Circadian Clock.* Cancer Discov, 2019. **9**(11): p. 1556-1573.
45. Park, S.Y., et al., *Inhibition of LEF1-Mediated DCLK1 by Niclosamide Attenuates Colorectal Cancer Stemness.* Clin Cancer Res, 2019. **25**(4): p. 1415-1429.
46. Dong, S., et al., *Chaperone-mediated autophagy sustains haematopoietic stem-cell function.* Nature, 2021. **591**(7848): p. 117-123.
47. Xu, Y., et al., *Chaperone-mediated autophagy regulates the pluripotency of embryonic stem cells.* Science, 2020. **369**(6502): p. 397-403.
48. Yang, Y., et al., *Emerging agents that target signaling pathways in cancer stem cells.* J Hematol Oncol, 2020. **13**(1): p. 60.
49. Lang, X., et al., *Radiotherapy and Immunotherapy Promote Tumoral Lipid Oxidation and Ferroptosis via Synergistic Repression of SLC7A11.* Cancer Discov, 2019. **9**(12): p. 1673-1685.
50. Liu, T., et al., *The Deubiquitylase OTUB1 Mediates Ferroptosis via Stabilization of SLC7A11.* Cancer Res, 2019. **79**(8): p. 1913-1924.
51. Dinallo, V., et al., *The Deubiquitinating Enzyme OTUD5 Sustains Inflammatory Cytokine Response in Inflammatory Bowel Disease.* J Crohns Colitis, 2022. **16**(1): p. 122-132.
52. Do, E.K., et al., *Kap1 regulates the self-renewal of embryonic stem cells and cellular reprogramming by modulating Oct4 protein stability.* Cell Death Differ, 2021. **28**(2): p. 685-699.
53. Cui, C.P., et al., *Author Correction: Dynamic ubiquitylation of Sox2 regulates proteostasis and governs neural progenitor cell differentiation.* Nat Commun, 2019. **10**(1): p. 173.
54. Wang, J., et al., *Ube2s regulates Sox2 stability and mouse ES cell maintenance.* Cell Death Differ, 2016. **23**(3): p. 393-404.
55. Wu, J., et al., *Intercellular interaction dictates cancer cell ferroptosis via NF2-YAP signalling.* Nature, 2019. **572**(7769): p. 402-406.
56. Koppula, P., L. Zhuang, and B. Gan, *Cystine transporter SLC7A11/xCT in cancer: ferroptosis, nutrient dependency, and cancer therapy.* Protein Cell, 2021. **12**(8): p. 599-620.

Figures

Figure 1

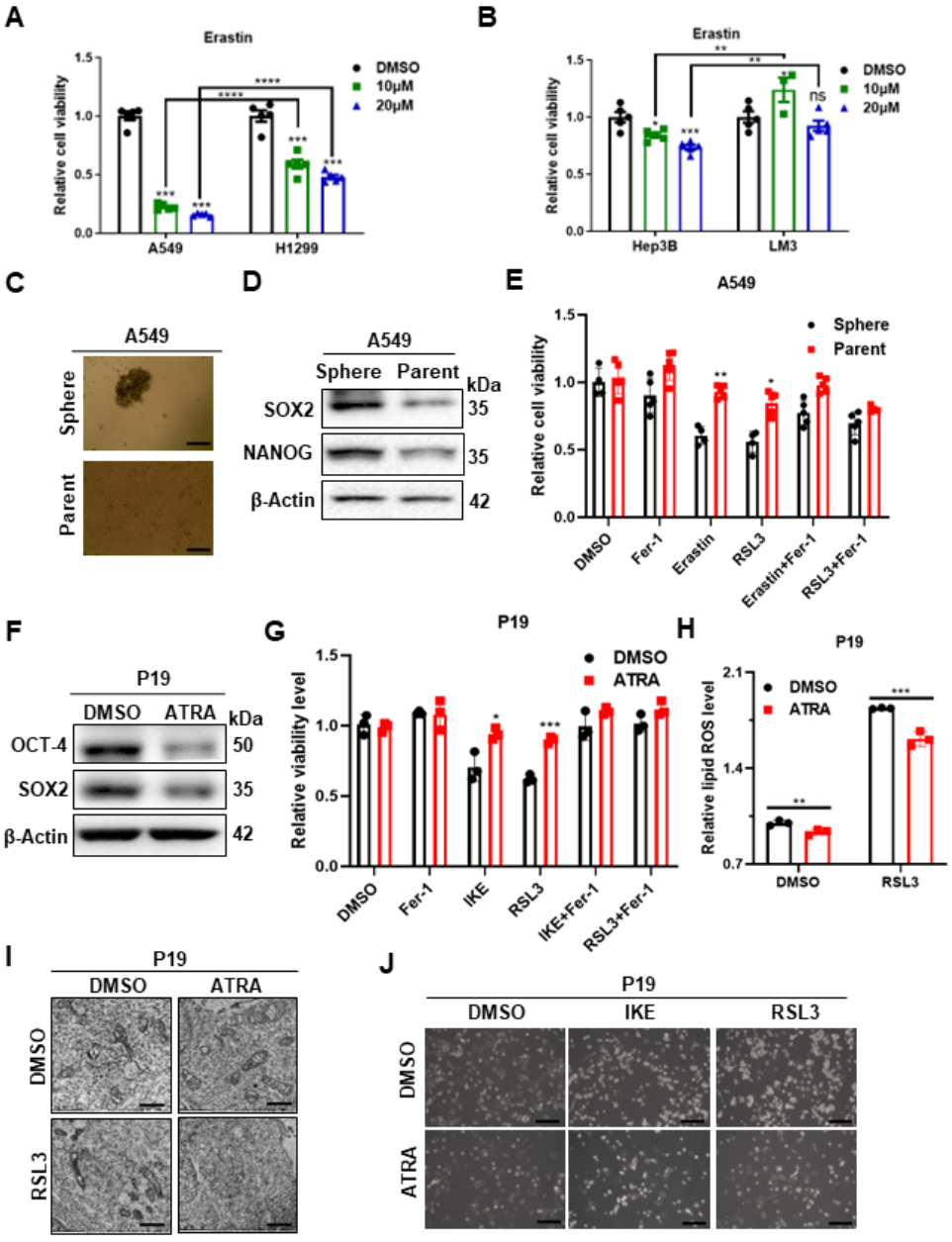

Figure 1

Undifferentiated cells are more sensitive to ferroptosis than differentiated cells.

A The viability of A549 cells and H1299 cells treated with erastin for the indicated concentrations was counted by CCK-8.

B The viability of Hep3B cells and LM3 cells treated with erastin for the indicated concentrations was counted by CCK-8.

C Representative images of A549 cells and A549 oncospheres. Scale bar, 100 μm.

D Stemness-related proteins were detected by western blotting in A549 cells and A549 oncospheres.

E The viability of A549 cells and A549 oncospheres treated with erastin, RSL3, and Fer-1 was counted by CCK-8.

F Stemness-related proteins were detected by western blotting in P19 cells and P19 cells treated with ATRA for 48 hours.

G The viability of P19 cells and ATRA-induced P19 cells treated with erastin, RSL3, and Fer-1 was counted by CCK-8.

H The lipid ROS level of P19 cells and ATRA-induced P19 cells treated with RSL3 was analyzed by flow cytometry using the probe BODIPY® 581/591.

I Representative mitochondrion pictures in P19 cells and ATRA-induced P19 cells treated with RSL3 were assessed by transmission electron microscope. Scale bar, 2 μm.

J Representative images of P19 cells and ATRA-induced P19 cells treated with IKE

and RSL3. Scale bar, 100 μm.

Figure 2

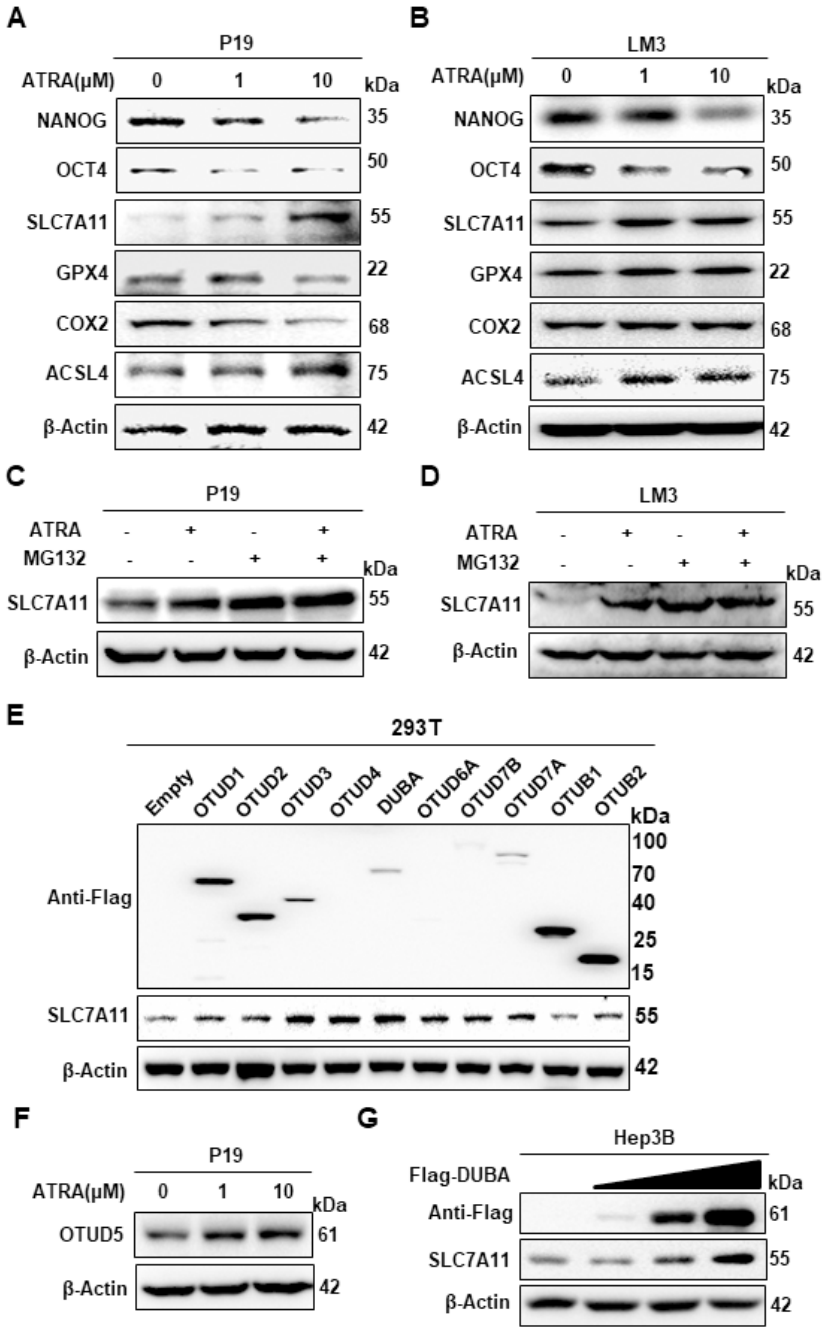

Figure 2

SLC7A11 is up-regulated by DUBA in differentiated cells.

A Stemness- and ferroptosis-related proteins were detected by western blotting in P19 cells treated with ATRA for the indicated concentrations.

B Stemness- and ferroptosis-related proteins were detected by western blot in LM3 cells treated with ATRA for the indicated concentrations.

C The protein levels of SLC7A11 were detected by western blotting in P19 cells which were treated with ATRA for 48 hours and then treated with MG132.

D The protein levels of SLC7A11 were detected by western blotting in P19 cells which were treated with ATRA for 48 hours and then treated with MG132.

E The indicated OTU subfamily DUBs were each transfected into 293T cells and SLC7A11 expression was detected by western blotting.

F DUBA was detected by western blotting in P19 cells treated with ATRA for the indicated concentrations.

G Increasing amounts of DUBA were transfected into Hep3B cells and the protein levels of SLC7A11 were detected by western blotting.

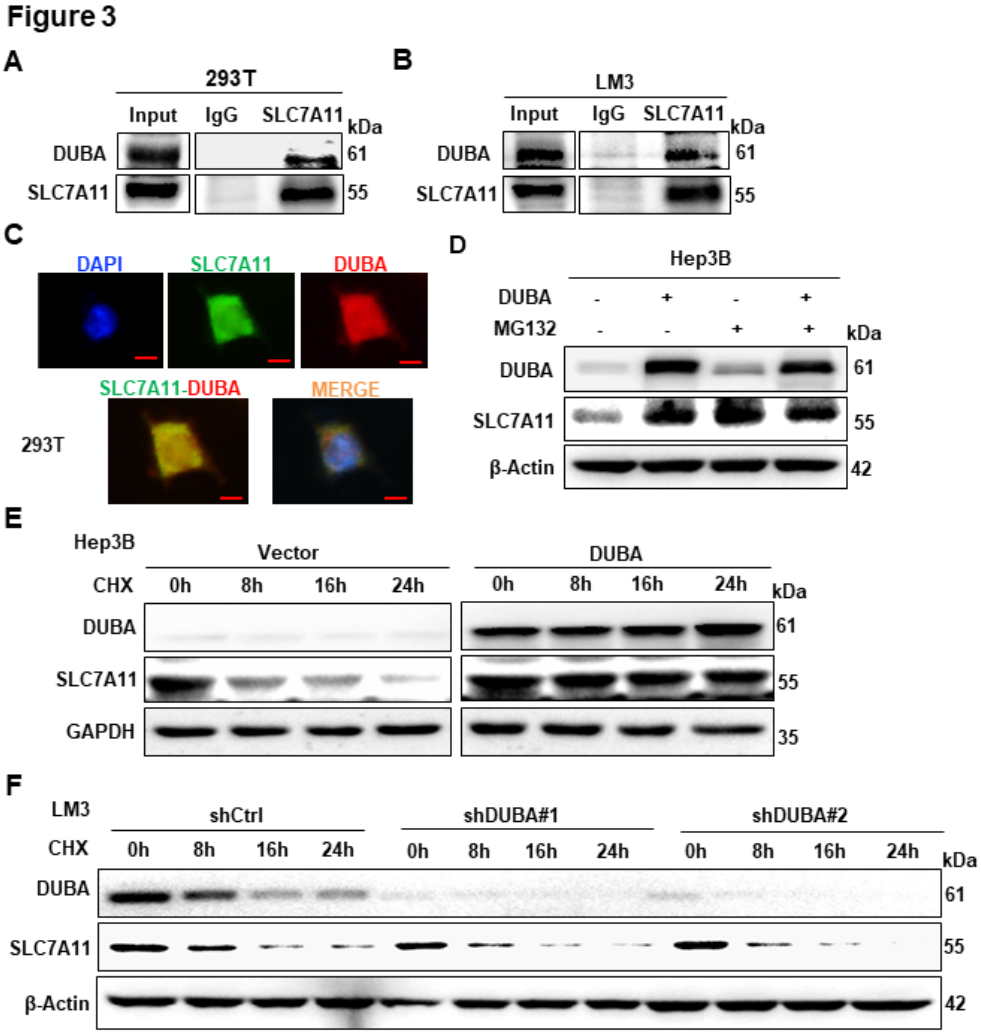

Figure 3

DUBA stabilizes and interacts with SLC7A11.

A 293T cells were co-transfected with DUBA and SLC7A11, and the cell lysates were subject to immunoprecipitation with control IgG and anti-SLC7A11 antibodies.

B Hep3B cell lysates were subject to immunoprecipitation with control IgG and anti-SLC7A11 antibodies.

C Immunofluorescent staining of DUBA and SLC7A11 in 293T cells co-transfected with DUBA and SLC7A11.

D SLC7A11 expression was detected by western blotting in DUBA-overexpressed

Hep3B cells treated with MG132.

E SLC7A11 expression was detected by western blotting in DUBA-overexpressed

Hep3B cells treated with CHX for the indicated hours.

F SLC7A11 expression was detected by western blotting in DUBA- knockdown

LM3 cells treated with CHX for the indicated hours.

Figure 4

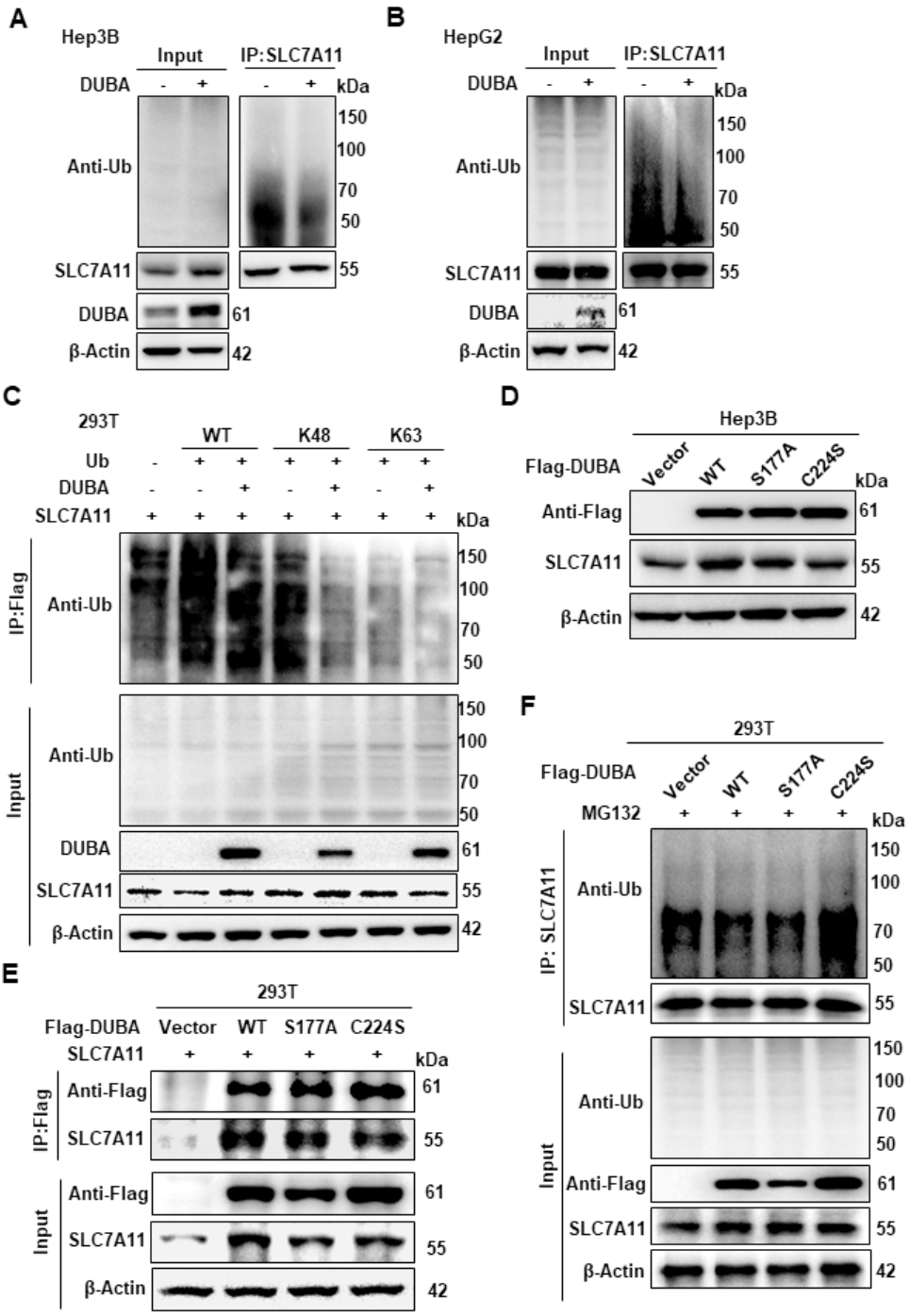

Figure 4

DUBA deubiquitinates SLC7A11.

A DUBA-overexpressed Hep3B cells were treated with MG132. And the cell lysates were subject to immunoprecipitate with anti-SLC7A11 antibody, which was followed by immunoblot with anti-Ub antibody to detect SLC7A11 ubiquitination.

B DUBA-overexpressed HepG2 cells were treated with MG132. And the cell lysates were subject to immunoprecipitate with anti-SLC7A11 antibody, which was followed by immunoblot with anti-Ub antibody to detect SLC7A11 ubiquitination.

C SLC7A11, HA-Ub, or its lysine residue K48 and K63 were transfected into 293T cells with or without Flag-DUBA which were treated with MG132. The cell lysates were immunoprecipitated with anti-SLC7A11 antibody, which was followed by immunoblot with anti-Ub antibody to detect SLC7A11 ubiquitination.

D Hep3B cells were transfected with Flag-tagged DUBA WT, DUBA S177A, or DUBA C224S mutants. And SLC7A11 expression was detected by western blotting.

E 293T cells were transfected with SLC7A11 alone or in combination with Flag-tagged DUBA WT, DUBA S177A, or DUBA C224S mutants. And the cell lysates were subject to immunoprecipitation with an anti-SLC7A11 antibody.

F Flag-tagged DUBA WT, DUBA S177A, or DUBA C224S mutants were transfected into 293T cells treated with MG132. And the cell lysates were subject to immunoprecipitation with an anti-SLC7A11 antibody.

Figure 5

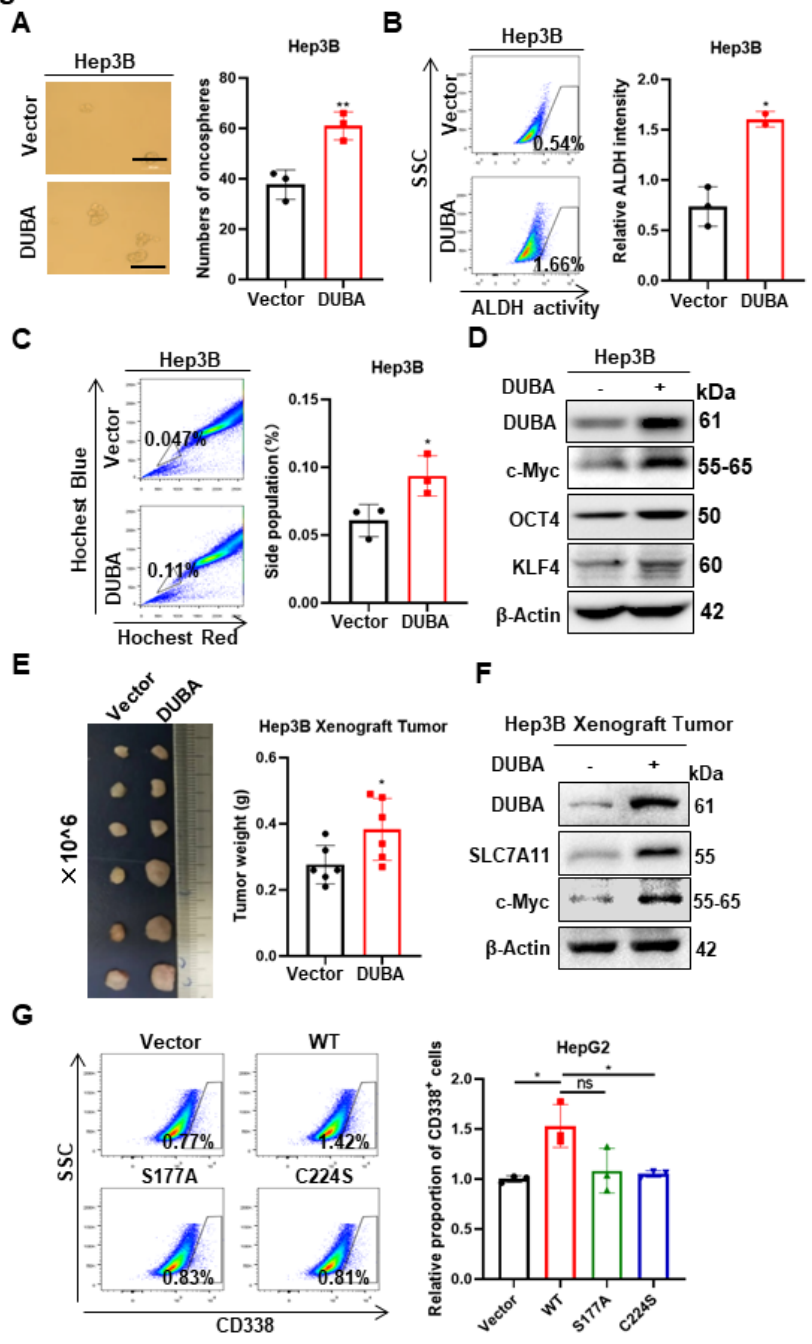

Figure 5

DUBA inhibits cell ferroptosis and enhances cell stemness.

A Representative oncosphere pictures of Hep3B cells stably expressing DUBA was taken (left), and the numbers of oncospheres were recorded in the bar graph (right).

B Representative images of ALDH activity in Hep3B cell stably expressing DUBA were analyzed by flow cytometry using the dye ALDEFLUOR (left). And the ALDH intensity was calculated in the bar graph (right).

C Representative images of SP cells in Hep3B cell stably expressing DUBA were analyzed by flow cytometry using the dye Hoechst 33342 (left). And the percentage of SP cells was calculated in the bar graph (right).

D Stemness-related proteins were detected by western blotting in Hep3B cells stably expressing DUBA.

E Tumor pictures (left) of mice with subcutaneous injection of DUBA-overexpressed Hep3B cells with limiting dilution were taken, and tumor weight was recorded in the bar graph (right).

F Stemness-related proteins were detected by western blotting in Hep3B xenograft tumors from (E).

G Representative images of CD338 positive cells in HepG2 cell with DUBA WT, DUBA S177A, and DUBA C224S mutants were analyzed by flow cytometry using CD338 antibody (left). And the percentage of CD338 positive cells was calculated in the bar graph (right).

Figure 6

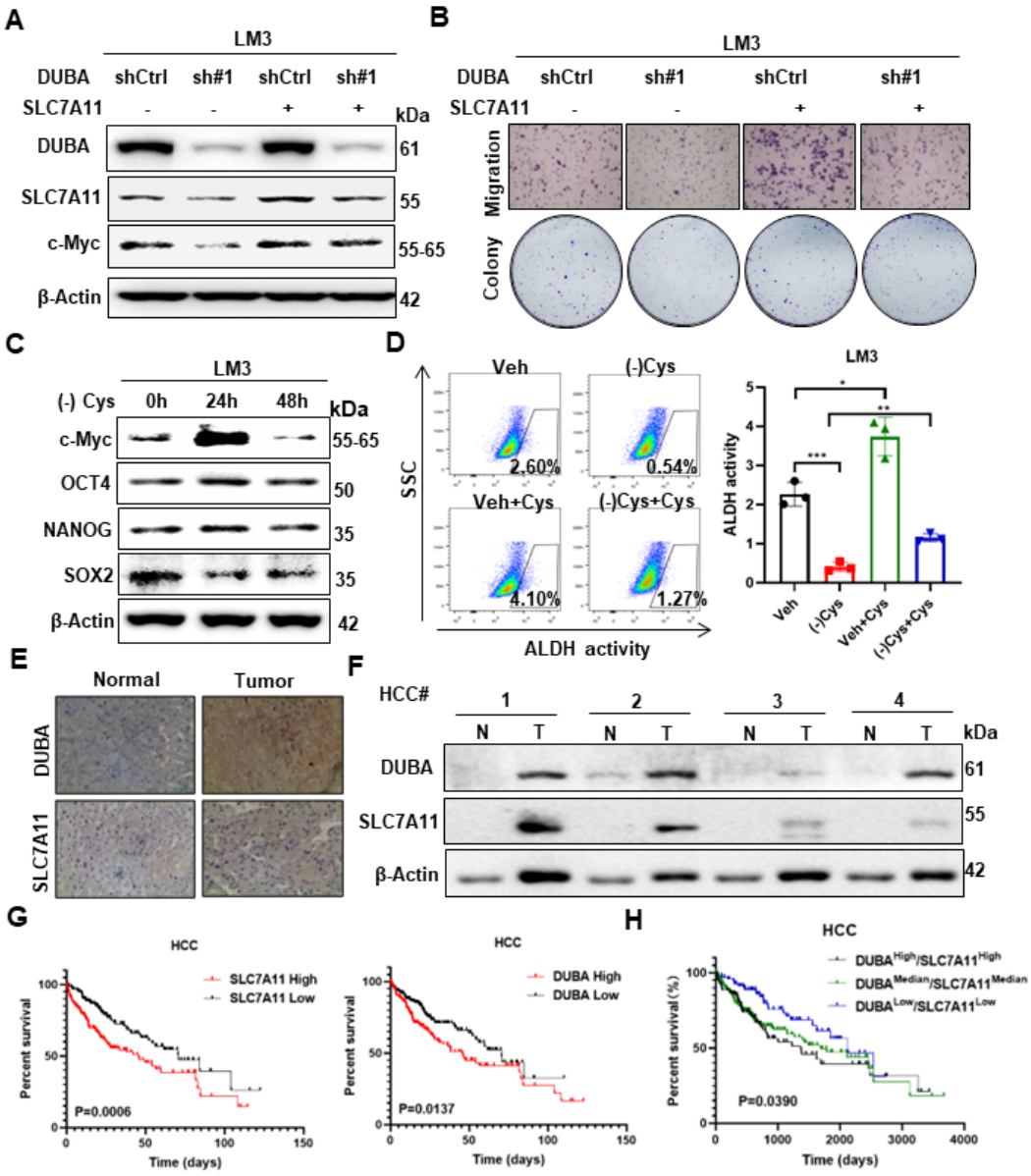

Figure 6

The DUBA-SLC7A11-c-Myc axis enhances stemness and predicts a poor prognosis in HCC Patients.

A DUBA-knockdown LM3 cells using shRNA#1 were transfected with SLC7A11.

B Representative images of cell migration and colony were derived from **(A)**.

C LM3 cells were cultured in DMEM medium lacking cystine for the indicated hours, and stemness-related proteins were detected by western blotting.

D Representative images of ALDH activity in LM3 cells cultured in DMEM medium lacking cysteine were analyzed by flow cytometry using the dye ALDEFLUOR (left). And the ALDH intensity was calculated in the bar graph (right).

E Representative IHC images of DUBA and SLC7A11 in normal tissue and tumor tissue derived from HCC patients (Normal n=10; Tumor n=10).

F DUBA and SLC7A11 expression was detected by western blotting in paracancerous tissue (N) and tumor tissue (T) derived from HCC patients

G Kaplan-Meier overall survival curves were compared between HCC patients with a high or low SLC7A11 level (left) and a high or low DUBA level (right) (High n=184; Low n=184).

H Kaplan-Meier overall survival curves were compared between HCC patients with a combined high expression of SLC7A11 and DUBA or an integrated low SLC7A11 level and low DUBA level (High n=94; Median n=188; Low n=94).

Figure 7

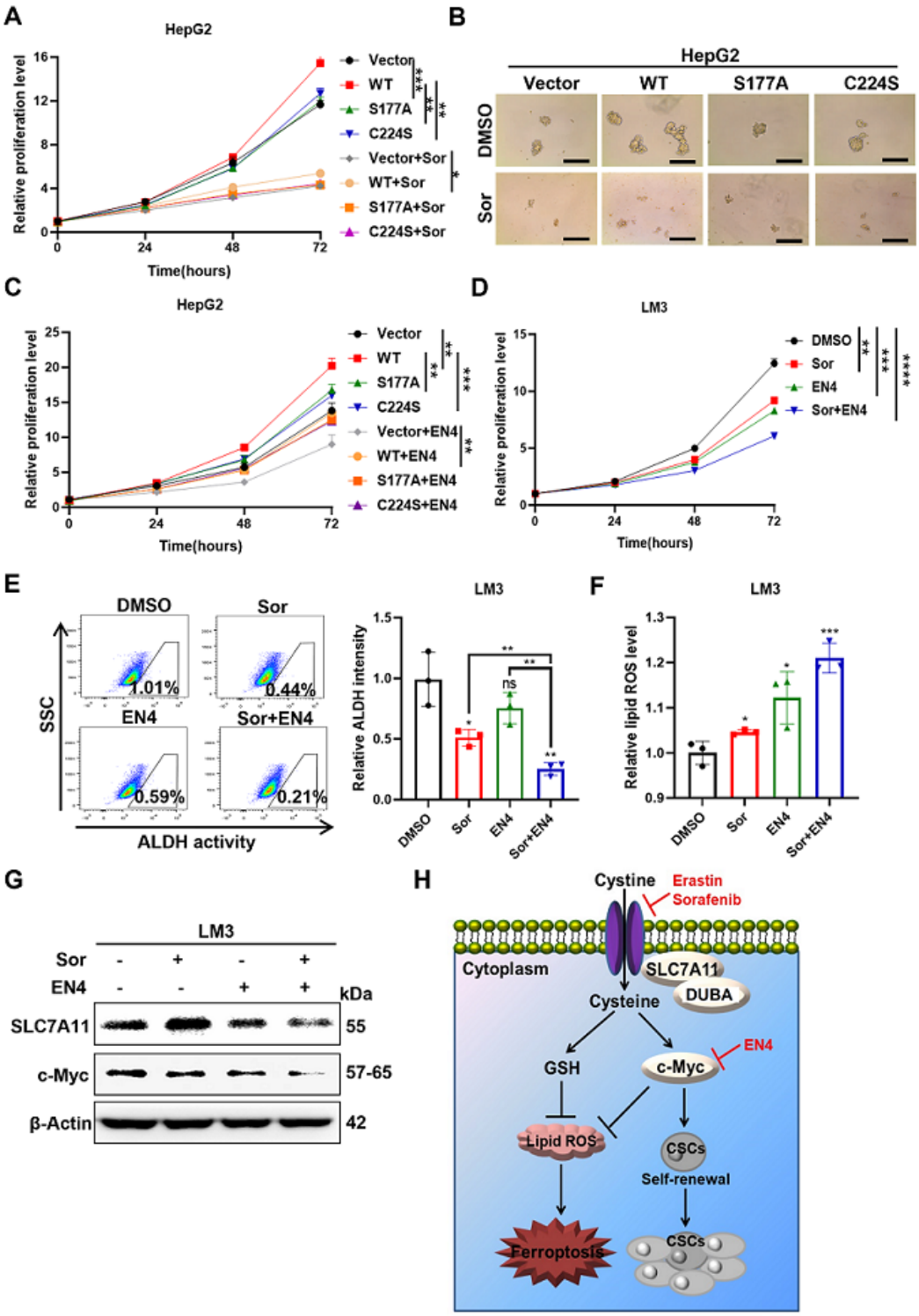

Figure 7

The combined treatment of sorafenib and c-Myc inhibitor EN4 inhibits HCC.

A The growth of HepG2 cells transfected with DUBA WT, DUBA S177A, and DUBA C244S mutants and treated with sorafenib was counted by CCK-8.

B Representative oncosphere and colony pictures of HepG2 cells transfected with DUBA WT, DUBA S177A, and DUBA C244S mutants and treated with sorafenib.

C The growth of HepG2 cells transfected with DUBA WT, DUBA S177A, and DUBA C244S mutants and treated with EN4 was counted by CCK-8.

D The growth of LM3 cells treated with sorafenib and EN4 was counted by CCK-8.

E Representative images of ALDH activity in LM3 cells treated with sorafenib or EN4 alone, and in combination with sorafenib and EN4, was analyzed by flow cytometry using the dye ALDEFLUOR (left). And the ALDH intensity was calculated in the bar graph (right).

F The lipid ROS level of LM3 cells treated with sorafenib or EN4 alone, and in combination with sorafenib and EN4, was analyzed by flow cytometry using the probe BODIPY® 581/591.

G SLC7A11 and c-Myc expression were detected by western blotting in LM3 cells treated with sorafenib or EN4 alone and in combination with sorafenib and EN4.

H A schematic model of DUBA-SLC7A11-c-Myc axis in ferroptosis inhibition and

stemness maintenance, increasing the resistance to sorafenib and EN4.

Supplementary Files

This is a list of supplementary files associated with this preprint. Click to download.

- SupplementaryInformation.docx